PERGAMON

International Journal of Solids and Structures 38 (2001) 3599–3613

INTERNATIONAL JOURNAL OF SOLIDS and STRUCTURES

www.elsevier.com/locate/ijsolstr

Static and dynamic analyses of tensegrity structures. Part 1. Nonlinear equations of motion

Hidenori Murakami *

Department of Mechanical and Aerospace Engineering, University of California at San Diego, 9500 Gilman Drive, La Jolla, CA 92093-0411, USA

Received 12 April 1999; in revised form 30 May 2000

Abstract

In order to present basic equations for static and dynamic analyses of a class of truss structures called tensegrity structures, large-deformation kinematics and kinetics were presented in both Eulerian and Lagrangian formulations. The two sets of equations of motion yield the same values even if different stress and strain measures were employed for their computation. The Eulerian formulation was implemented in an updated Lagrangian finite element code using Newton's method with consistently linearized equations of motion. By utilizing the linearized Lagrangian equations of motion at pre-stressed initial configurations, harmonic modal analyses of a three-bar tensegrity module and a six-stage tensegrity beam were conducted. In the second part of the paper, linearized equations were utilized to investigate the equilibrium configurations of basic tensegrity modules and the stiffness of pre-stressed tensegirty structures.

Keywords: Tensegrity; Nonlinear truss analysis; Pre-stress

1. Introduction

Tensegrity is a class of truss structures, which consist of pin-jointed tension and compression members. According to Marks and Fuller (1973) and Pugh (1976), tensegrity consists of discontinuous bars or compression members suspended by a continuous network of cables or pure tension members. The tensegrity structure was invented by Kenneth Snelson in 1948 (Schultz, 1981). Buckminster Fuller named Snelson's structure "tensegrity" and conglomerated tensegrity domes by extending his concept of geodesic domes (Marks and Fuller, 1973). In a recent article on tensegrity, Ingber (1998) illustrated a wide variety of natural systems from nano to mega scales, which are assembled with the tensegrity architecture.

The class of tensegrity structures investigated in this paper exhibits "inferior order of stiffness" noted by Clerk Maxwell (1864, 1890) if

$$\mathrm{M}x \equiv n_{\mathrm{E}} - n_{\mathrm{V}} \leqslant 0, \tag{1}$$

* Tel.: +1-858-534-3821; fax: +1-858-534-4543.
E-mail address: murakami@mae.ucsd.edu (H. Murakami).

0020-7683/01/$ - see front matter
PII: S0020-7683(00)00232-8

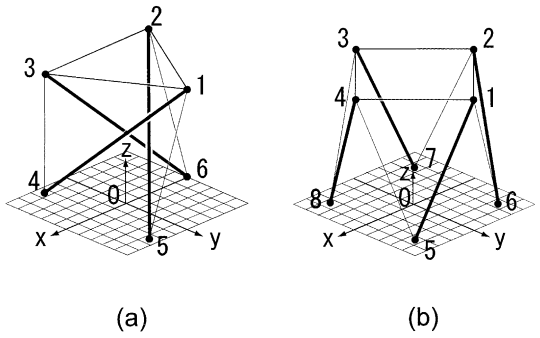

Fig. 1. Cyclic cylindrical (a) three-bar and (b) four-bar tensegrity modules.

where Mx is referred to as the Maxwell number, n_E is the number of elements, and n_V is the number of unknown degrees-of-freedom after constraining a truss against rigid body motion. Fig. 1(a) and (b) illustrate a three-bar cyclic cylindrical tensegrity module and a four-bar module, investigated by Tarnai (1980). The base and top nodes form equilateral triangles in Fig. 1(a) and squares in Fig. 1(b). The top triangle and square are twisted with respect to the base triangle and square by $\pi/2 + \pi/3$ and $\pi/2 + \pi/4$, respectively, in the counterclockwise direction from the position where the bars are vertical. In the figure, thick lines denote bars while thin lines illustrate cables. When the pre-stressed modules were subjected to vertical loads in the negative z-direction, the initial response was soft and accompanied by large deformation of swinging bars in the counterclockwise direction. As the loads increased, the stiffness of the load–displacement curve quadratically increased. An initial deformation mode was referred to as "infinitesimal mechanisms" (Calladine, 1978; Tarnai, 1980; Pellegrino and Calladine, 1986) and was resisted by the stiffness on the order of pre-stress.

A recent trend in smart structural systems is to endow flexible structures with control engineering (Skelton and Sultan, 1997). In this endeavor, infinitesimal mechanisms of tensegrity structures have become an advantage for deployable and shape-controlled structures for easy manipulation (e.g. Motro, 1990; Furuya, 1992; Hanaor, 1993). Controlled tensegrity structures (Skelton and Sultan, 1997) achieve smartness by control systems, thereby extending the applications of smart structures.

A majority of previous works on the mechanics of tensegrity structures benefited from the large deformation analysis of pre-stressed cable networks by Argyris and Scharpf (1972). Cable networks are similar to tensegrity structures in their need for finding initial geometry and pre-stress modes. However, they differ in geometrical arrangements.

The objective of this paper is to furnish basic equations for both static and dynamic analyses of tensegrity structures based on large deformation kinematics and kinetics of trusses. For this purpose, the equations of motion are developed both in Eulerian formulation at the current configuration and in Lagrangian formulation with reference to a pre-stressed initial configuration. (The Eulerian and Lagrangian formulations are often referred to as the spatial and material formulations, respectively.) Linearized equations of motion are used to conduct modal analyses of a three-bar tensegrity module and a tensegrity beam. All linear models developed for various applications of tensegrity structures are only valid in the neighborhood of a reference configuration at which linear equations are obtained. Therefore, it is important that all linear models share the same basic assumptions and are consistently expanded. In the present approach, all linear models are derived from the same nonlinear truss equations. In the second part of this paper, the linear and nonlinear equilibrium equations are employed to investigate pre-stress modes, infinitesimal mechanism modes, and stiffness of cylindrical tensegrity modules.

2. Deformation kinematics

A motion of a truss structure with n_N nodes in Euclidean space $\mathbf{R}^3$ is described by the nodal coordinates $\mathbf{x}_G(t)$ with respect to an inertial Cartesian coordinate system $\{x_1, x_2, x_3\}$ and time t. The global node numbers, $1, 2, \ldots, n_N$, identify the nodes of the entire truss structure, while local nodes $\hat{1}$ and $\hat{2}$ identify the end nodes of each truss element, as illustrated in Figs. 1 and 2. A relationship between the global and local node numbers for each element establishes the element connections. Let n_E denote the total number of truss elements. The union of centroidal axes of truss elements, $\Omega_0^{(e)}$, $e = 1, 2, \ldots, n_E$, in a pre-stressed reference configuration at time $t = 0$ is denoted by Ω_0. At time t, the deformed current centroidal axes occupy region Ω_t consisting of the truss elements $\Omega_t^{(e)}$, $e = 1, 2, \ldots, n_E$. To establish the evolution of $\mathbf{x}_G(t)$, one needs the nodal velocities, $\mathbf{w}_G(t)$, which are governed by the conservation laws.

Let a material point $\mathbf{X}$ on $\Omega_0^{(e)}$ deform to $\mathbf{x}$ on $\Omega_t^{(e)}$, as shown in Fig. 2. The deformation is expressed by the mapping

$$\mathbf{x} = \mathbf{x}(\mathbf{X}, t). \tag{2}$$

The mapping is also defined by introducing the displacement field $\mathbf{u}(\mathbf{X}, t)$ as

$$\mathbf{x}(\mathbf{X}, t) = \mathbf{X} + \mathbf{u}(\mathbf{X}, t). \tag{3}$$

The straight centroidal axis of each truss element is assumed to remain straight under large translation and rotation involving uniaxial tension or compression.

Let the rectangular Cartesian coordinate system attached to the cylinder of truss element (e) in the reference configuration $\Omega_0^{(e)}$ be denoted by $\{\Theta_1, \Theta_2, \Theta_3\}^{(e)}$, where Θ_1 denotes the length coordinate of the centroidal axis and the Θ_2, Θ_3-plane defines the plane of cross-section. The axial direction of element (e) is denoted by $\mathbf{G}^{(e)} \equiv (\mathrm{d}\mathbf{X}/\mathrm{d}\Theta_1)^{(e)}$ with the unit vector pointing from local node $\hat{1}$ to node $\hat{2}$. The mass density, area of cross-section, and length of $\Omega_0^{(e)}$ are denoted by $\rho_0^{(e)}$, $A_0^{(e)}$, and $l_0^{(e)}$, respectively. The mass per unit axial length is $m_0^{(e)} \equiv (\rho_0 A_0)^{(e)}$. An infinitesimal truss volume element is expressed as $\mathrm{d}V_0^{(e)} = (\rho_0 A_0 \mathrm{d}\Theta_1)^{(e)}$.

In truss elements, it is assumed that each cross-section normal to the centroidal axis remains normal during deformation. Therefore, in the current deformed configuration $\Omega_t^{(e)}$, the convected $\{\Theta_1, \Theta_2, \Theta_3\}^{(e)}$ coordinate system remains orthogonal. Let the rectangular Cartesian coordinate system aligned with the convected coordinate system be denoted by $\{\theta_1, \theta_2, \theta_3\}^{(e)}$. The $\theta_1^{(e)}$-coordinate is the length parameter of the centroidal axis $\Omega_t^{(e)}$. The axial direction of element (e) is denoted by $\mathbf{g}^{(e)} \equiv (\mathrm{d}\mathbf{x}/\mathrm{d}\theta_1)^{(e)}$ with the unit vector pointing from local node $\hat{1}$ to node $\hat{2}$. The deformation gradient $\mathbf{F}$ of (2) with respect to the $\{\theta_1, \theta_2, \theta_3\}^{(e)}$ and $\{\Theta_1, \Theta_2, \Theta_3\}^{(e)}$ coordinate systems is expressed in terms of principal stretches:

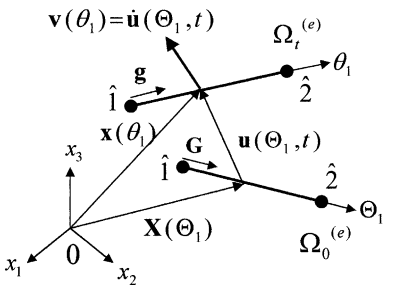

Fig. 2. A truss element in the current and reference configurations.

$$\mathbf{F} = \begin{bmatrix} \frac{\mathrm{d}\theta_1}{\mathrm{d}\Theta_1} & 0 & 0 \\ 0 & \frac{\mathrm{d}\theta_2}{\mathrm{d}\Theta_2} & 0 \\ 0 & 0 & \frac{\mathrm{d}\theta_3}{\mathrm{d}\Theta_3} \end{bmatrix}, \tag{4}$$

where $\mathrm{d}\theta_2/\mathrm{d}\Theta_2 = \mathrm{d}\theta_3/\mathrm{d}\Theta_3$ in each plane of cross-section.

The mass density, area of cross-section, and length of $\Omega_t^{(e)}$ are denoted by $\rho_t^{(e)}$, $A_t^{(e)}$, and $l_t^{(e)}$, respectively. The mass per unit axial length is $m_t^{(e)} \equiv (\rho_t A_t)^{(e)}$. An infinitesimal truss volume element is $\mathrm{d}V_t^{(e)} = (\rho_t A_t \mathrm{d}\theta_1)^{(e)}$.

Let superposed dots and $\mathrm{D}/\mathrm{D}t$ signify the material time differentiation by holding $\mathbf{X}$. The velocity field of $\Omega_t^{(e)}$ is expressed by $\mathbf{v}^{(e)}(\theta_1)$ defined on $\Omega_t^{(e)}$ or $\dot{\mathbf{u}}^{(e)}(\Theta_1)$ defined on $\Omega_0^{(e)}$. In the sequel, it becomes necessary to compute div $\mathbf{v}$ on the centroidal axis. The computation of div $\mathbf{v}$ on the centroidal axis requires a consistent approximation of the velocity field on each cross-section with the three-dimensional conservation laws. Therefore, basic truss equations are derived from those of the three-dimensional theory of elasticity. The following three-dimensional kinematical relations are utilized (Marsden and Hughes, 1983):

$$\mathrm{d}V_t = J\mathrm{d}V_0, \qquad \dot{J} = J\mathrm{div}\,\mathbf{v}, \tag{5a, b}$$

in which J is the Jacobian. For a truss element the Jacobian becomes

$$J^{(e)} = \left(\frac{A_t}{A_0}\right)^{(e)} \left(\frac{\mathrm{d}\theta_1}{\mathrm{d}\Theta_1}\right)^{(e)}. \tag{6a}$$

By taking the material time derivatives of Eq. (6a) and using Eq. (5b), one obtains the material time derivative of the cross sectional area A_t:

$$\dot{A}_t^{(e)} = A_t^{(e)}(\mathrm{div}\,\mathbf{v} - d_{11})^{(e)}, \tag{6b}$$

where d_{11} is the axial stretch-rate defined on $\Omega_t^{(e)}$ as

$$d_{11} = \frac{\mathrm{d}\mathbf{v}}{\mathrm{d}\theta_1} \cdot \mathbf{g} = \frac{\mathrm{d}v_1}{\mathrm{d}\theta_1}, \tag{6c}$$

in which $v_1 = \mathbf{v} \cdot \mathbf{g}$ is the axial velocity component. It is noted that Eq. (6b) furnishes the value of div $\mathbf{v}$ on the centroidal axis in terms of d_{11} and A_t without explicitly approximating the velocity field on each cross-section.

3. Conservation of mass

The three-dimensional conservation of mass is written as

$$\rho_t J = \rho_0, \qquad \dot{\rho}_t + \rho_t \mathrm{div}\,\mathbf{v} = 0, \tag{7a, b}$$

where Eq. (7a) is expressed with respect to $\mathbf{X}$ for the Lagrangian (material) formulation, while Eq. (7b) is expressed with respect to $\mathbf{x}$ for the Eulerian (spatial) formulation. From Eq. (7a), the conservation of mass for an infinitesimal truss element is obtained as

$$m_t^{(e)} \left(\frac{\mathrm{d}\theta_1}{\mathrm{d}\Theta_1}\right)_t^{(e)} = m_0^{(e)}. \tag{8a}$$

If the stretch ratio, $\mathrm{d}\theta_1/\mathrm{d}\Theta_1$, is uniform over the element, Eq. (8a) can be integrated to yield

$$(m_t l_t)^{(e)} = (m_0 l_0)^{(e)}. \tag{8b}$$

The spatial form of Eq. (8a) is obtained from Eq. (7b), $m_t \equiv \rho_t A_t$, and Eq. (6b) as follows:

$$\dot{m}_t^{(e)} + (m_t d_{11})^{(e)} = 0. \tag{8c}$$

4. Elastic constitutive equations

In this paper, truss elements are characterized as nonlinearly elastic materials. Three-dimensional elastic response under isothermal deformation is described by using the Helmholtz free energy per unit mass, Ψ, in terms of the second Piola–Kirchhoff stress tensor $\mathbf{S}$ and the Lagrangian strain tensor $\mathbf{E}$ (e.g., Marsden and Hughes, 1983):

$$\mathbf{S} = \rho_0 \frac{\partial \Psi}{\partial \mathbf{E}}, \tag{9a}$$

in which $\mathbf{E}$ is defined in terms of the deformation gradient $\mathbf{F}$ and the 3×3 identity matrix $\mathbf{I}_3$ as

$$\mathbf{E} \equiv \tfrac{1}{2}(\mathbf{F}^{\mathrm{T}}\mathbf{F} - \mathbf{I}_3), \tag{9b}$$

where $(\ )^{\mathrm{T}}$ signifies the transpose of $(\ )$. Both $\mathbf{S}$ and $\mathbf{E}$ are defined on the reference configuration Ω_0.

The rate form of Eq. (9a) becomes

$$\dot{\mathbf{S}} = \underline{\underline{\mathbf{C}}} : \dot{\mathbf{E}}, \tag{9c}$$

where $\underline{\underline{\mathbf{C}}}$ is the fourth-order elastic modulus tensor:

$$\underline{\underline{\mathbf{C}}} \equiv \rho_0 \frac{\partial \Psi}{\partial \mathbf{E} \partial \mathbf{E}}. \tag{9d}$$

Eqs. (9a)–(9d) are defined on the reference configuration and are utilized for the Lagrangian formulation. For the Eulerian formulation, the above relations are expressed in terms of the Cauchy stress tensor $\boldsymbol{\sigma}$ and its Truesdell rate, $\boldsymbol{\sigma}^*$, defined on the current configuration, (for the derivation in terms of the vector-valued Cauchy stress two-form used by Brillouin (1964), see the Appendix of Frankel (1997)). The relationship between the second Piola–Kirchhoff stress tensor $\mathbf{S}$ and the Cauchy stress tensor $\boldsymbol{\sigma}$ defined on Ω_t is

$$\boldsymbol{\sigma} = \frac{1}{J}\mathbf{F}\mathbf{S}\mathbf{F}^{\mathrm{T}}. \tag{10a}$$

The rate constitutive relation, (9c), transforms to

$$\boldsymbol{\sigma}^* = \underline{\underline{\mathbf{c}}} : \mathbf{d}, \tag{10b}$$

where $\mathbf{d}$ is the rate of deformation tensor and $\underline{\underline{\mathbf{c}}}$ is the Piola transform of the elastic modulus tensor $\underline{\underline{\mathbf{C}}}$ (Hughes and Pister, 1978; Marsden and Hughes, 1983):

$$\underline{\underline{\mathbf{c}}} = \frac{1}{J}\mathbf{F}\mathbf{F}\mathbf{F}\mathbf{F}\underline{\underline{\mathbf{C}}}. \tag{10c}$$

Since it is assumed that truss elements are under uniaxial tension or compression, stress components other than S_{11} or σ_{11} vanish. For elastic truss elements, Eq. (9a) reduces to

$$S_{11}A_0 = m_0 \frac{\mathrm{d}\Psi}{\mathrm{d}E_{11}}, \tag{11a}$$

where the axial Lagrangian strain E_{11} is defined as

$$\mathrm{d}\mathbf{x} \cdot \mathrm{d}\mathbf{x} - \mathrm{d}\mathbf{X} \cdot \mathrm{d}\mathbf{X} = (\mathrm{d}\theta_1)^2 - (\mathrm{d}\Theta_1)^2 \equiv 2E_{11}(\mathrm{d}\Theta_1)^2. \tag{11b}$$

The rate form of Eq. (11a) is expressed as

$$\dot{S}_{11}A_0 = Y_0A_0\dot{E}_{11}, \tag{12a}$$

where the tangent elastic modulus Y_0A_0 is defined as

$$Y_0A_0 = m_0\frac{\mathrm{d}^2\Psi}{\mathrm{d}E_{11}^2}. \tag{12b}$$

For linearly elastic materials, Y_0 is independent of E_{11} and becomes Young's modulus. For truss elements, relation (10a) reduces to

$$\sigma_{11}A_t = S_{11}A_0\left(\frac{\mathrm{d}\theta_1}{\mathrm{d}\Theta_1}\right)_t. \tag{13}$$

Under uniaxial stress condition, the rate relation (10b) reduces to

$$\sigma_{11}^* \equiv \dot{\sigma}_{11} + \sigma_{11}(\mathrm{div}\,\mathbf{v} - 2d_{11}) = Y_td_{11}, \tag{14a}$$

where the current axial stiffness is

$$Y_tA_t = Y_0A_0\left(\frac{\mathrm{d}\theta_1}{\mathrm{d}\Theta_1}\right)_t^3. \tag{14b}$$

From Eqs. (14a,b) and (6b), the material time derivative of the axial resultant force is expressed as

$$\frac{\mathrm{D}}{\mathrm{D}t}(\sigma_{11}A_t) = (Y_t + \sigma_{11})A_td_{11}. \tag{15}$$

Eq. (15) is also derived from Eq. (12a) and the material time derivative of Eq. (13).

5. Eulerian equations of motion

The position vector $\mathbf{x}$ and the velocity vector $\mathbf{v}$ constitute basic kinematic variables in the Eulerian formulation. The kinematics of a truss structure are described by using 3 $n_\mathrm{N} \times 1$ nodal coordinate vector $\mathbf{x}_\mathrm{G}(t)$, nodal velocity vector $\mathbf{w}_\mathrm{G}(t)$, and nodal acceleration vector $\dot{\mathbf{w}}_\mathrm{G}(t)$. The nodal acceleration is governed by the equations of motion. In the sequel, components of all nodal vectors are defined with respect to the global coordinate system $\{x_1, x_2, x_3\}$.

To obtain the equations of motion, consider a free-body-diagram of an infinitesimal line element $\Delta\theta_1$ of $\Omega_t^{(e)}$ illustrated in Fig. 3. In the figure, $\mathbf{g}^{(e)} \equiv (\mathrm{d}\mathbf{x}/\mathrm{d}\theta_1)^{(e)}$ denotes a unit axial vector. The infinitesimal element is subjected to the Cauchy traction $(\sigma_{11}A_t\mathbf{g})^{(e)}$ and the external resultant force per unit axial length, $(m_t\mathbf{b})^{(e)}$, due to both lateral surface traction and body forces. Newton's second law applied to the infinitesimal element in Fig. 3 facilitates

$$\frac{\mathrm{d}}{\mathrm{d}\theta_1}(\sigma_{11}A_t\mathbf{g})^{(e)} + (m_t\mathbf{b})^{(e)} = (m_t\dot{\mathbf{v}})^{(e)}, \tag{16}$$

where $\dot{\mathbf{v}}$ is the acceleration vector.

The traction boundary condition at node j subjected to a concentrated nodal force $\mathbf{f}_j$ is expressed as

$$\sum_{e_j}(-1)^{\hat{j}+1}(\sigma_{11}A_t\mathbf{g})^{(e_j)} = \mathbf{f}_j \quad j = 1, 2, \ldots, n_\mathrm{V}, \tag{17}$$

in which the summation is over the elements which meet at node j. In Eq. (17), the sign of $\mathbf{g}^{(e)}$ is -1, if node j in element (e) is local node $\hat{1}$ and $+1$, if node j is local node $\hat{2}$.

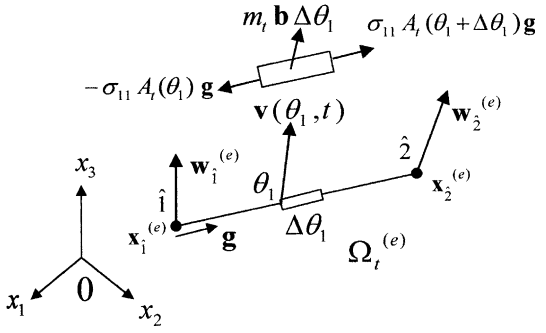

Fig. 3. Eulerian kinematics and kinetics of a deformed truss element.

To transform Eq. (16) and the nodal traction boundary conditions (17) into the principle of virtual work or velocity on the current configuration Ω_t, a one-parameter family of admissible deformation $\delta\mathbf{v}$ is introduced by freezing time t. Virtual velocity components vanish on the boundary, if the corresponding velocity components are prescribed. Let $n_v \times 1$ column matrices $\mathbf{w}$ and $\delta\mathbf{w}$ represent unknown nodal-values of the velocity field $\mathbf{v}$ and the corresponding virtual velocity field $\delta\mathbf{v}$ defined on Ω_t. The prescribed nodal velocities with $n_C \equiv 3\,n_N - n_V$ components are not included in $\mathbf{w}$, but they are included in $\mathbf{w}_G$.

The principle of virtual work becomes

$$\sum_{e=1}^{n_E}\int_0^{l_t^{(e)}}\{\delta d_{11}\sigma_{11}A_t - \delta\mathbf{v}\cdot m_t(\mathbf{b}-\dot{\mathbf{v}})\}^{(e)}\mathrm{d}\theta_1^{(e)} - \delta\mathbf{w}\cdot\mathbf{f}_N = 0, \tag{18a}$$

where d_{11} is the stretch rate defined by Eq. (6c), δd_{11} denotes the virtual stretch rate:

$$\delta d_{11}^{(e)} = \left(\frac{\mathrm{d}}{\mathrm{d}\theta_1}\delta\mathbf{v}\cdot\mathbf{g}\right)^{(e)}, \tag{18b}$$

and $\mathbf{f}_N$ is an $n_V \times 1$ column matrix, whose elements describe the nodal concentrated forces. By substituting Eq. (18b) into Eq. (18a) and integrating by parts, one obtains Eq. (16) on $\Omega_t^{(e)}$ and the traction boundary conditions (17) at each node as the Euler–Lagrange equations.

Let 6×1 matrices $\mathbf{w}^{(e)}$ and $\delta\mathbf{w}^{(e)}$ denote, respectively, nodal velocities and virtual nodal velocities of element (e), each storing the ith velocity components of local node $\hat{1}$ in the ith element and that of local node $\hat{2}$ in the $(i+3)$rd element. Both the velocity and virtual velocity fields on $\Omega_t^{(e)}$ are linearly interpolated by using $\mathbf{w}^{(e)}$ and $\delta\mathbf{w}^{(e)}$, respectively, as

$$\mathbf{v}^{(e)}(\theta_1) = \mathbf{N}^{(e)}\mathbf{w}^{(e)}, \qquad \delta\mathbf{v}^{(e)}(\theta_1) = \mathbf{N}^{(e)}\delta\mathbf{w}^{(e)}, \tag{19a, b}$$

where $\mathbf{N}^{(e)}$ is the 3×6 interpolation matrix defined as

$$\mathbf{N}^{(e)} \equiv [\,N_1(\theta_1)\mathbf{I}_3 \quad N_2(\theta_1)\mathbf{I}_3\,]^{(e)}, \tag{19c}$$

in which $N_1(\theta_1)$ and $N_2(\theta_1)$ are shape functions:

$$N_1^{(e)}(\theta_1) \equiv 1 - \left(\frac{\theta_1}{l_t}\right)^{(e)}, \qquad N_2^{(e)}(\theta_1) \equiv \left(\frac{\theta_1}{l_t}\right)^{(e)}. \tag{19d, e}$$

The substitution of Eqs. (19a)–(19d) into Eq. (18a) with Eq. (18b) yields

$$\sum_{e=1}^{n_E} \delta \mathbf{w}^{(e)} \cdot \left[\mathbf{M}^{(e)} \dot{\mathbf{w}}^{(e)} + \mathbf{p}^{(e)} - \mathbf{f}_b^{(e)} \right] - \delta \mathbf{w} \cdot \mathbf{f}_N = 0, \tag{20a}$$

where $\mathbf{M}^{(e)}$, $\mathbf{p}^{(e)}$, and $\mathbf{f}_b^{(e)}$ denote, respectively, the element mass matrix, the element internal force vector, and the element external force vector due to the distributed body force $(m_t \mathbf{b})^{(e)}$:

$$\mathbf{M}^{(e)} \equiv \frac{1}{6} (m_t l_t)^{(e)} \begin{bmatrix} 2\mathbf{I}_3 & \mathbf{I}_3 \\ \mathbf{I}_3 & 2\mathbf{I}_3 \end{bmatrix}, \tag{20b}$$

$$\mathbf{p}^{(e)} \equiv \begin{Bmatrix} -\mathbf{g} \\ \mathbf{g} \end{Bmatrix}^{(e)} (\sigma_{11} A_t)^{(e)}, \tag{20c}$$

$$\mathbf{f}_b^{(e)} \equiv \int_0^{l_t^{(e)}} \mathbf{N}^{(e)^T} (m_t \mathbf{b})^{(e)} \mathrm{d}\theta_1^{(e)}. \tag{20d}$$

The global-to-local mapping from $\mathbf{w}$ in $\mathbf{R}^{n_V}$ to $\mathbf{w}^{(e)}$ in $\mathbf{R}^6$ as well as $\delta\mathbf{w}$ in $\mathbf{R}^{n_V}$ to $\delta\mathbf{w}^{(e)}$ in $\mathbf{R}^6$ is expressed by an $n_V \times 6$ matrix, $\mathbf{L}g^{(e)}$, whose rows consist of the natural unit vectors $\mathbf{e}_1, \mathbf{e}_2, \ldots, \mathbf{e}_{n_V}$ in $\mathbf{R}^{n_V}$:

$$\mathbf{w}^{(e)} = \mathbf{L}g^{(e)} \mathbf{w}, \qquad \delta\mathbf{w}^{(e)} = \mathbf{L}g^{(e)} \delta\mathbf{w}. \tag{21a, b}$$

For example, if the jth component of the element velocity vector $\mathbf{w}^{(e)}$ is the ith component of the global velocity vector $\mathbf{w}$, then the jth row of $\mathbf{L}g^{(e)}$ becomes the transpose of $\mathbf{e}_i$ in $\mathbf{R}^{n_V}$ (e.g., LM array of Hughes, 1987). The same global-to-local projection is used between the global and elemental internal-force vectors, $\mathbf{p}$ and $\mathbf{p}^{(e)}$, and the global and elemental body-force vectors, $\mathbf{f}_b$ and $\mathbf{f}_b{}^{(e)}$. By using Eqs. (21a,b), Eq. (20a) is expressed in global quantities as

$$\delta\mathbf{w} \cdot \left[\mathbf{M}\dot{\mathbf{w}} + \mathbf{p} - \mathbf{f} \right] = 0, \tag{22a}$$

where

$$\mathbf{f} \equiv \mathbf{f}_N + \mathbf{f}_b, \tag{22b}$$

and the assembled global quantities are defined as

$$\mathbf{M} \equiv \sum_{e=1}^{n_E} \mathbf{L}g^{(e)^T} \mathbf{M}^{(e)} \mathbf{L}g^{(e)}, \tag{22c}$$

$$\mathbf{p} \equiv \sum_{e=1}^{n_E} \mathbf{L}g^{(e)^T} \mathbf{p}^{(e)}, \tag{22d}$$

$$\mathbf{f}_b \equiv \sum_{e=1}^{n_E} \mathbf{L}g^{(e)^T} \mathbf{f}_b^{(e)}. \tag{22e}$$

Since $\delta\mathbf{w}$ is arbitrary, one obtains the FE equations of motion expressed on the current configuration Ω_t:

$$\mathbf{M}\dot{\mathbf{w}} + \mathbf{p} - \mathbf{f}(t) = 0, \tag{23}$$

where $\mathbf{M}$ is the global mass matrix, $\mathbf{p}$ is the internal force vector, and $\mathbf{f}$ is the external force vector. Viscous damping forces, if they exist, are included in $\mathbf{p}$. A well-posed initial value problem is defined by Eq. (23) with Eqs. (22b)–(22e), (15) and (14b), and prescribed time evolution of $\mathbf{f}(t)$, as well as the initial conditions at time $t = 0$ for $\mathbf{w}(0)$ and $\mathbf{x}_G(0)$. Tensegrity structural analysis and design differ from those of simple and compound spatial trusses. Designers must find a self-equilibrium configuration and choose the amplitude of

a pre-stress mode. In the first part of the paper, it is assumed that the initial configuration and pre-stresses are prescribed. The initial equilibrium analysis of basic tensegrity modules will be presented in the second part of the paper.

An updated Lagrangian code was developed by using the Newmark method for the time integration of Eq. (23) (e.g., Bathe, 1982; Hughes, 1987). The integration scheme presented by Hughes and Winget (1980) was employed for integrating Eq. (15). Further, to achieve a second-order convergence rate in iterations between t and $t + \Delta t$, Newton's method was used. This method requires the definition for the residual force, which is the left-hand side of Eq. (23), and the consistently linearized equation of Eq. (23) to find improved approximation (Hughes and Pister, 1978). The derivation of linearized equations of Eq. (23) with respect to a pre-stressed configuration is deferred to the next section. The updated Lagrangian code was used to investigate the stability and stiffness of tensegrity modules in the second part of the paper. In the code, if the compressive force of a cable element exceeded a critical load during shortening, the tangent stiffness associated with the compressive force was reduced to $10^{-6}(Y_0 + \sigma_{11})$ to mimic cable slacking (Murakami et al., 1998).

Let $\mathbf{s}(0)$ be the $n_{\mathrm{E}} \times 1$ column matrix of the initial element forces, whose eth element is $(\sigma_{11}A_t)^{(e)} = (S_{11}A_0)^{(e)}$ at $t = 0$. The initial equilibrium equation (23) reduces to

$$\mathbf{p}(0) = \mathbf{A}\mathbf{s}(0) = \mathbf{0}, \tag{24a}$$

where the $n_{\mathrm{V}} \times n_{\mathrm{E}}$ equilibrium matrix $\mathbf{A}$ at $t = 0$ is defined from Eqs. (20c) and (22d) as

$$\mathbf{A} \equiv \lfloor\, \mathbf{a}_1 \quad \mathbf{a}_2 \quad \cdots \quad \mathbf{a}_{n_{\mathrm{E}}} \,\rfloor, \tag{24b}$$

$$\mathbf{a}_e \equiv \mathbf{L} g^{(e)\mathrm{T}} \begin{Bmatrix} -\mathbf{g} \\ \mathbf{g} \end{Bmatrix}^{(e)}. \tag{24c}$$

In Eq. (24c), the nonzero entries of the eth column of $\mathbf{A}$ consist of the direction cosines, $\mathbf{g}^{(e)} = \mathbf{G}^{(e)}$ at $t = 0$. The initial equilibrium Eq. (24a) holds without any assumptions. However, if the external force $\mathbf{f}$ is placed on the right-hand side of Eq. (24a), the resulting equilibrium equation with $\mathbf{A}$, defined by Eq. (24c) at $t = 0$, holds only for small deformations.

6. Lagrangian equations of motion

For Newton's method and modal analyses, linearized equations of motion with respect to a pre-stressed state are required. The basic equations are facilitated here in the Lagragian or material formulation. The deformed configuration $\Omega_t^{(e)}$ at time t is described by the displacement field $\mathbf{u}^{(e)}(\Theta_1, t)$ defined on the reference element $\Omega_0^{(e)}$ at $t = 0$, whose axial-length is parameterized by Θ_1. The basic kinematic variables of the Lagrangian formulation are $\mathbf{u}$ and $\dot{\mathbf{u}}$. The kinematics of a truss is, therefore, described in terms of the initial nodal coordinate vector $\mathbf{X}_{\mathrm{G}}$, the unknown nodal displacement vector $\mathbf{d}$, and the nodal velocity vector $\dot{\mathbf{d}}$. The equations of motion render $\ddot{\mathbf{d}}$ from which $\dot{\mathbf{d}}$ and $\mathbf{d}$ are computed by time integration. The current nodal position vector is obtained by using Eq. (3) as $\mathbf{x}_{\mathrm{G}} = \mathbf{X}_{\mathrm{G}} + \mathbf{d}_{\mathrm{G}}$.

The Lagrangian strain E_{11} is obtained from Eq. (11b) as

$$E_{11} = \mathbf{G} \cdot \frac{\mathrm{d}\mathbf{u}}{\mathrm{d}\Theta_1} + \frac{1}{2} \frac{\mathrm{d}\mathbf{u}}{\mathrm{d}\Theta_1} \cdot \frac{\mathrm{d}\mathbf{u}}{\mathrm{d}\Theta_1}, \tag{25a}$$

by using

$$\mathrm{d}\mathbf{x}^{(e)} = \mathbf{g}^{(e)} \mathrm{d}\theta_1^{(e)} = \left(\mathbf{G} + \frac{\mathrm{d}\mathbf{u}}{\mathrm{d}\Theta_1} \right)^{(e)} \mathrm{d}\Theta_1^{(e)}, \tag{25b}$$

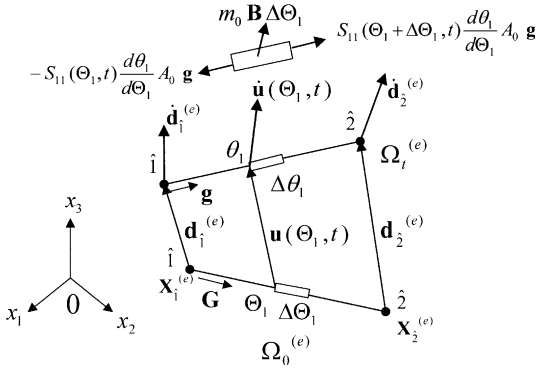

Fig. 4. Lagrangian kinematics and kinetics of a deformed truss element $\Omega_t^{(e)}$ with reference to the reference truss element $\Omega_0^{(e)}$ at $t=0$.

$$\mathrm{d}\mathbf{X}^{(e)}=\frac{\mathrm{d}\mathbf{X}}{\mathrm{d}\Theta_1}\mathrm{d}\Theta_1^{(e)}=\mathbf{G}^{(e)}\mathrm{d}\Theta_1^{(e)}. \tag{25c}$$

The Lagrangian equations of motion are obtained by expressing on $\Omega_0^{(e)}$ the Cauchy traction $(\sigma_{11}A_t)^{(e)}$ and the body force $(m_t\mathbf{b})^{(e)}$, which are defined on $\Omega_t^{(e)}$ by using the deformation map (3). The Cauchy traction $(\sigma_{11}A_t)^{(e)}$ defined on $\Omega_t^{(e)}$ is expressed in terms of the first Piola–Kirchhoff stress P_{11} or the second Piola–Kirchhoff stress S_{11} by using the Piola transformation (Marsden and Hughes, 1983; Frankel, 1997):

$$(P_{11}A_0)^{(e)}=\left(\frac{\mathrm{d}\theta_1}{\mathrm{d}\Theta_1}\right)^{(e)}(S_{11}A_0)^{(e)}=(\sigma_{11}A_t)^{(e)}. \tag{26}$$

In Eq. (26), both $(P_{11}A_0)^{(e)}$ and $(S_{11}A_0)^{(e)}$ are defined on $\Omega_0^{(e)}$, while $(\sigma_{11}A_t)^{(e)}$ is defined on $\Omega_t^{(e)}$. The body force term is easily expressed on $\Omega_0^{(e)}$ as $\mathbf{B}(\Theta_1,t)=\mathbf{b}(\theta_1(\Theta_1))$. Newton's second law applied to the free-body-diagram in Fig. 4 renders the Lagrangian equations of motion

$$\left\{\frac{\mathrm{d}}{\mathrm{d}\Theta_1}\left(\frac{\mathrm{d}\theta_1}{\mathrm{d}\Theta_1}S_{11}A_0\mathbf{g}\right)\right\}^{(e)}+(m_0\mathbf{B})^{(e)}=(m_0\ddot{\mathbf{u}})^{(e)}. \tag{27}$$

To express Eq. (18a) on Ω_0, d_{11} and δd_{11} are expressed by $\dot{E}_{11}$ and $\delta\dot{E}_{11}$ respectively as

$$d_{11}=\frac{\mathrm{d}\dot{\theta}_1}{\mathrm{d}\theta_1}=\dot{E}_{11}\left(\frac{\mathrm{d}\Theta_1}{\mathrm{d}\theta_1}\right)^2,\quad \delta d_{11}=\frac{\mathrm{d}\delta\dot{\theta}_1}{\mathrm{d}\theta_1}=\delta\dot{E}_{11}\left(\frac{\mathrm{d}\Theta_1}{\mathrm{d}\theta_1}\right)^2. \tag{28a, b}$$

Eq. (28a) is obtained by taking the material time derivatives of Eq. (11b).

By using Eqs. (26) and (28a), one finds the following relations for the strain-energy rate and the virtual strain-energy rate:

$$(S_{11}\dot{E}_{11}A_0\mathrm{d}\Theta_1)^{(e)}=(\sigma_{11}d_{11}A_t\mathrm{d}\theta_1)^{(e)}, \tag{29a}$$

$$(S_{11}\delta\dot{E}_{11}A_0\mathrm{d}\Theta_1)^{(e)}=(\sigma_{11}\delta d_{11}A_t\mathrm{d}\theta_1)^{(e)}. \tag{29b}$$

A one-parameter family of admissible deformation on $\Omega_t^{(e)}$ with respect to $\Omega_0^{(e)}$ is described by the virtual velocity field $\delta\dot{\mathbf{u}}^{(e)}$. The nodal values of $\delta\dot{\mathbf{u}}^{(e)}$ are represented by the virtual nodal velocity vector $\delta\dot{\mathbf{d}}$. The principle of virtual work expressed on Ω_0 becomes

$$\sum_{e=1}^{n_E}\int_0^{l_0^{(e)}}\{\delta\dot{E}_{11}S_{11}A_0-\delta\dot{\mathbf{u}}\cdot m_0(\mathbf{B}-\ddot{\mathbf{u}})\}^{(e)}\mathrm{d}\Theta_1^{(e)}-\delta\dot{\mathbf{d}}\cdot\mathbf{f}_N=0. \tag{30a}$$

If one takes the material time-derivative of Eq. (11b) with Eqs. (25b,c), the strain rate and velocity relation is found

$$\dot{E}_{11} = \left(\mathbf{G} + \frac{\mathrm{d}\mathbf{u}}{\mathrm{d}\Theta_1}\right)^{(e)} \cdot \frac{\mathrm{d}\dot{\mathbf{u}}}{\mathrm{d}\Theta_1}, \qquad \delta\dot{E}_{11} = \left(\mathbf{G} + \frac{\mathrm{d}\mathbf{u}}{\mathrm{d}\Theta_1}\right)^{(e)} \cdot \frac{\mathrm{d}\delta\dot{\mathbf{u}}}{\mathrm{d}\Theta_1}. \tag{30b, c}$$

By using Eq. (30c), one can show that Eq. (30a) yields Eq. (27) and the nodal traction boundary conditions (17) expressed on $\Omega_0^{(e)}$ by using Eq. (26) as the Euler–Lagrange equations.

In the Lagrangian formulation, both $\dot{\mathbf{u}}$ and $\delta\dot{\mathbf{u}}$ are linearly interpolated on $\Omega_0^{(e)}$ by using nodal velocity $\dot{\mathbf{d}}^{(e)}$ and virtual nodal velocity $\delta\dot{\mathbf{d}}^{(e)}$, respectively, as

$$\dot{\mathbf{u}}^{(e)}(\Theta_1^{(e)}, t) = \mathbf{N}_L^{(e)}\dot{\mathbf{d}}^{(e)}, \qquad \delta\dot{\mathbf{u}}^{(e)}(\Theta_1^{(e)}, t) = \mathbf{N}_L^{(e)}\delta\dot{\mathbf{d}}^{(e)}, \tag{31a, b}$$

where $\mathbf{N}_L^{(e)}$ is the 3×6 interpolation matrix:

$$\mathbf{N}_L^{(e)} \equiv [\, N_1(\Theta_1)\mathbf{I}_3 \quad N_2(\Theta_1)\mathbf{I}_3 \,]^{(e)}, \tag{31c}$$

and the shape functions, $N_1(\Theta_1)$ and $N_2(\Theta_2)$, are defined on $\Omega_0^{(e)}$ as

$$N_1^{(e)}(\Theta_1^{(e)}) \equiv 1 - \left(\frac{\Theta_1}{l_0}\right)^{(e)}, \qquad N_2^{(e)}(\Theta_1^{(e)}) \equiv \left(\frac{\Theta_1}{l_0}\right)^{(e)}. \tag{31d, e}$$

In Eqs. (31a,b), the first three components of $\dot{\mathbf{d}}^{(e)}$ and $\delta\dot{\mathbf{d}}^{(e)}$ are those for local node $\hat{1}$, while the remaining three components are those for local node $\hat{2}$. The strain rate and the virtual strain rates (30b,c) become

$$\dot{E}_{11}^{(e)} = \mathbf{B}^{(e)}\dot{\mathbf{d}}^{(e)}, \qquad \delta\dot{E}_{11}^{(e)} = \mathbf{B}^{(e)}\delta\dot{\mathbf{d}}^{(e)}, \tag{32a, b}$$

where

$$\mathbf{B}^{(e)} \equiv \frac{1}{l_0^{(e)}}\left[\, -\mathbf{G}^{\mathrm{T}} \quad \mathbf{G}^{\mathrm{T}} \,\right]^{(e)} + \left(\frac{1}{l_0^{(e)}}\right)^2 \mathbf{d}^{(e)^{\mathrm{T}}} \begin{bmatrix} \mathbf{I}_3 & -\mathbf{I}_3 \\ -\mathbf{I}_3 & \mathbf{I}_3 \end{bmatrix}. \tag{32c}$$

In the second part of the paper, the second term on the right-hand side of Eq. (32c) will be used to explain the hardening response of tensegrity modules with increasing mechanism-mode displacements.

For the linear interpolation (31a)–(31e), the deformation map (3) on $\Omega_0^{(e)}$ yields

$$\left(\frac{\theta_1}{l_t}\right)^{(e)} = \left(\frac{\Theta_1}{l_0}\right)^{(e)}. \tag{33}$$

By substituting Eqs. (31a)–(32b) into Eq. (30a), one finds

$$\sum_{e=1}^{n_{\mathrm{E}}} \delta\dot{\mathbf{d}}^{(e)} \cdot \left[\mathbf{M}_L^{(e)}\ddot{\mathbf{d}}^{(e)} + \mathbf{p}_L^{(e)} - \mathbf{f}_{bL}^{(e)}\right] - \delta\dot{\mathbf{d}} \cdot \mathbf{f}_{\mathrm{N}} = 0, \tag{34a}$$

where $\mathbf{M}_L^{(e)}$, $\mathbf{p}_L^{(e)}$, and $\mathbf{f}_{bL}^{(e)}$ are defined as

$$\mathbf{M}_L^{(e)} \equiv \frac{1}{6}(m_0 l_0)^{(e)} \begin{bmatrix} 2\mathbf{I}_3 & \mathbf{I}_3 \\ \mathbf{I}_3 & 2\mathbf{I}_3 \end{bmatrix}, \tag{34b}$$

$$\mathbf{p}_L^{(e)} \equiv \left[\left\{ \begin{array}{c} -\mathbf{G} \\ \mathbf{G} \end{array} \right\}^{(e)} + \frac{1}{l_0^{(e)}} \begin{bmatrix} \mathbf{I}_3 & -\mathbf{I}_3 \\ -\mathbf{I}_3 & \mathbf{I}_3 \end{bmatrix} \mathbf{d}^{(e)}\right] S_{11}^{(e)}(t) A_0^{(e)}, \tag{34c}$$

$$\mathbf{f}_{bL}^{(e)} \equiv \int_0^{l_0^{(e)}} \mathbf{N}_L^{(e)^{\mathrm{T}}} (m_0 \mathbf{B})^{(e)} \mathrm{d}\Theta_1^{(e)}. \tag{34d}$$

By using Eqs. (8b), (26), (32) and (25b) with Eq. (31), it can be easily shown that the values of $\mathbf{M}_L^{(e)}$, $\mathbf{p}_L^{(e)}$, and $\mathbf{f}_{bL}^{(e)}$ in Eqs. (34b)–(34d) are equal to those of $\mathbf{M}^{(e)}$, $\mathbf{p}^{(e)}$, and $\mathbf{f}_b^{(e)}$ in Eqs. (20b)–(20d).

The global-to-local projection, e.g., from $\dot{\mathbf{d}}$ in $\mathbf{R}^{n_V}$ to $\dot{\mathbf{d}}^{(e)}$ in $\mathbf{R}^6$ is defined in a similar manner to Eq. (21a,b). By assembling elemental quantities for global quantities by using $\mathbf{L}g^{(e)}$, the Lagrangian FE equations of motion are obtained:

$$\mathbf{M}_L\ddot{\mathbf{d}} + \mathbf{p}_L(t) - \mathbf{f}_L(t) = 0, \tag{35}$$

where the values of the mass matrix, the internal force vector, and the external force vector are identical to those in Eq. (23). However, Eqs. (23) and (35) differ in their domains of definition as well as in the stress and deformation measures employed for their computation.

When an element experiences large rigid-body translation and rotation involving nodal displacements on the order of element length, the calculation of the second term on the right-hand side of Eq. (34c) causes the subtraction of two similar numbers and triggers numerical divergence.

7. Linearized equations of motion

Let the pre-stressed state Ω_0 at $t = 0$ be a reference state with pre-stress $S_{11}^{(e)}(0)$. The pre-stress may approximately satisfy the initial equilibrium with the residual force $\zeta(0) \equiv \mathbf{f}(0) - \mathbf{p}(0)$. By utilizing the consistent linearization method presented by Hughes and Pister (1978), Eq. (35) can be linearlized for small nodal displacement vector $\mathbf{d}(t)$ on Ω_0 as

$$\mathbf{M}_L\ddot{\mathbf{d}} + \mathbf{K}_T\mathbf{d} - \mathbf{f}_L(t) = \zeta(0), \tag{36a}$$

where the symmetric tangent stiffness matrix $\mathbf{K}_T$ is defined as

$$\mathbf{K}_T \equiv \sum_{e=1}^{n_E} \mathbf{L}g^{(e)^T}\mathbf{K}_T^{(e)}\mathbf{L}g^{(e)}, \tag{36b}$$

$$\mathbf{K}_T^{(e)} \equiv \left(\frac{Y_0A_0}{l_0}\right)^{(e)}\begin{bmatrix}\mathbf{G}\mathbf{G}^T & -\mathbf{G}\mathbf{G}^T\\ -\mathbf{G}\mathbf{G}^T & \mathbf{G}\mathbf{G}^T\end{bmatrix}^{(e)} + \left(\frac{S_{11}(0)A_0}{l_0}\right)^{(e)}\begin{bmatrix}\mathbf{I}_3 & -\mathbf{I}_3\\ -\mathbf{I}_3 & \mathbf{I}_3\end{bmatrix}. \tag{36c}$$

The first term on the right-hand side of Eq. (36c) is the stiffness matrix used for small deformation analysis, while the second term denotes stiffening effects by pre-stresses. The elemental force increment from the pre-stressed configuration for small time increment Δt is computed by integrating Eqs. (12a), (32a) and (32c) with $\mathbf{d} = \mathbf{0}$. Similarly, the linearized equation (35) at time t is obtained by substituting $(Y_tA_t/l_t)^{(e)}$ for $(Y_0A_0/l_0)^{(e)}$, $\mathbf{g}_t^e$ for $\mathbf{G}^{(e)}$, $(\sigma_{11}(t)A_t/l_t)^{(e)}$ for $(S_{11}(0)A_0/l_0)^{(e)}$, and $\zeta(t)$ for $\zeta(0)$ in Eq. (36a–c).

Argyris and Scharpf (1972) derived the tangent stiffness matrix for small strain, but for large deformation problems. If Eq. (36c) is translated for small axial deformation, $\mathrm{d}\theta_1/\mathrm{d}\Theta_1 \approx 1$, using Eqs. (13), (14b) and (15), Eq. (22) of Argyris and Scharpf is recovered. They referred the first and the second terms of Eq. (36c) on the right-hand side as the "elastic" and "geometrical" forces, respectively. In Eq. (36c) the pre-stress stiffening effect is "isotropic" at each node due to its appearance through $\mathbf{I}_3$. For geometrically nonlinear analysis of kinematically determinate trusses without infinitesimal mechanisms, it is economical to employ the approximation of large deformation with "moderate rotation" (Przemieniecki, 1968). In the approximation, only nonlinear terms induced by transverse displacements are retained. This "inconsistent" linearization should not be used for tensegrity structures, since the model incorrectly exhibits anisotroic pre-stress stiffening instead of isotropic stiffening. It will be shown in the second part of the paper that the stiffness of infinitesimal mechanism displacements only comes from the second term on the right-hand side of Eq. (36c).

8. Dynamic analysis of tensegrity structures

The dynamic response of pre-stressed tensegrity structures can be investigated by conducting modal analyses. To this end, the linearized equations of motion (36a) is utilized. The tangent stiffness matrix defined by Eqs. (36b,c) includes the effect of pre-stress and is positive definite for tensegrity structures, which exhibit first-order infinitesimal mechanisms (Koiter, 1984). Consider a harmonic motion of the form $\mathbf{d} = \tilde{\mathbf{d}} \exp(\mathrm{i}\omega t)$, where $\tilde{\mathbf{d}}$ is the amplitude and ω is the angular frequency. The generalized FE eigenproblem is obtained from Eq. (36a) as

$$\mathbf{K}_{\mathrm{T}}\tilde{\mathbf{d}} = \omega^2 \mathbf{M}\tilde{\mathbf{d}}. \tag{37}$$

The above eigenproblem can be solved by either using the Lanczos method (Hughes, 1987) or the subspace iteration method (Bathe, 1982).

Modal analyses were conducted on a three-bar cylindrical tensegrity module in Fig. 1(a). For the numerical examples, bars and cables are assumed to be made of steel with Young's modulus $Y_0 = 200$ GPa and mass density $\rho = 7860$ kg/m^3. The geometrical properties are the radius of circumscribing circles 1 m, the height of the three-bar module 1 m, the radius of circular cylindrical cables 0.001 m, and the inner and outer radii of hollow circular cylindrical bars 0.018 and 0.022 m, respectively. The element force of the bar was changed from –200 to –1000 N. The corresponding compressive stress of the bar was between 0.4 and 1.99 MPa. Fig 5(a) and (b) illustrate by solid lines, the first and second modes of the three-bar tensegrity. The dashed lines show the initial pre-stressed configuration. The natural frequencies at the bar pre-stress −0.8 MPa are 1.49 and 35.00 Hz for the first and the second modes, respectively. To display complicated figures, each set of four figures include a perspective view in the first quadrant and three orthographic projections in the second, third, and fourth quadrants. The initial equilibrium analysis of the three-bar tensegrity module, presented in the second part of the paper, reveals that the static deformation is dominated by an infinitesimal mechanism mode of swinging bars in the counterclockwise direction. The first mode in Fig. 5(a) is almost identical to the infinitesimal mechanism mode, while deformation modes with nonzero element elongation appear as high frequency modes. The change of the natural frequencies with increasing values of bar pre-compression is shown in Table 1. The stiffness of the first mode is due to the pre-stress term in Eq. (36c), while the stiffness of the second, third and fourth modes are due to the axial stiffness and the pre-stress terms.

The modal analysis was also conducted on a six-stage tensegrity beam, illustrated in Fig. 6, which was built by stacking the three-bar modules with alternating twisting directions and by adding additional strings

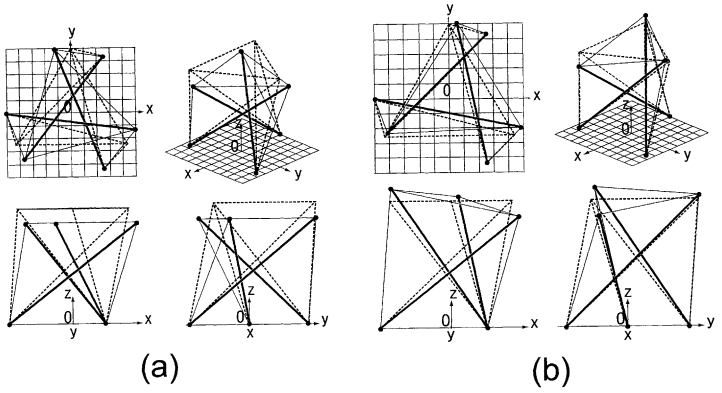

Fig. 5. (a) The first mode and (b) the second mode of the three-bar tensegrity module.

Table 1
The natural frequencies of the lowest four modes for various pre-stresses

Pre-stress of bars (MPa)	First mode (Hz)	Second mode (Hz)	Third mode (Hz)	Fourth mode (Hz)
0.40	1.05	34.99	34.99	68.44
0.80	1.49	35.00	35.00	68.45
1.19	1.83	35.01	35.01	68.46
1.59	2.11	35.03	35.03	68.47
1.99	2.36	35.04	35.04	68.47

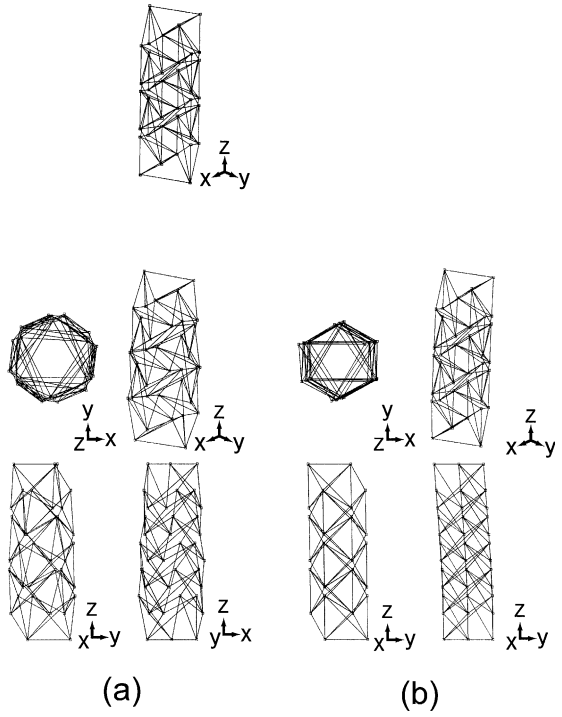

Fig. 6. (a) The first mode and (b) the second mode of a six-stage tensegrity beam.

(Skelton and Sultan, 1997; Murakami et al., 1998). The first and the second modes of the 6-stage tensegrity beam were shown in Fig. 6(a) and (b), respectively. It has been observed that the mechanism modes of three twisting bars in the direction of the twist angle are basic deformation mechanisms of the tensegrity beam. In the first mode in Fig. 6(a), the axial deformation of the beam is accomplished by adjacent counter-twisting sets of three bars. Therefore, the first mode is a globally longitudinal mode. The second mode in Fig. 6(b) appears as a flexural mode. The first mode represents an infinitesimal mechanism mode of the beam, and the natural frequency is much smaller than that of the second mode similar to the three-bar cylindrical tensegrity module.

9. Concluding remarks

In order to furnish a set of equations for static and dynamic analyses of tensegrity structures, equations of motion for spatial trusses were developed within the framework of three-dimensional theory of elasticity

for large deformation. It was found that the pre-stress stiffening effect appears isotropically in each node. In harmonic modal analysis near pre-stressed initial configurations, infinitesimal mechanisms were observed as the mode shape corresponding to the lowest natural frequency. The natural frequencies of infinitesimal mechanism modes increase proportionally to the square root of the amplitude of pre-stress. The natural frequencies of deformation modes with nonzero elastic force in Eq. (36c) do not change significantly with increasing pre-stress amplitudes.

Acknowledgements

The research was in part supported by the NASA Ames Research Center. The author would like to thank Professor Robert Skelton at University of California, San Diego (UCSD) for stimulating discussions on tensegrity structures. The author is deeply indebt to Professor Emeritus Theodore Frankel at UCSD for his valuable advice and guidance in differential geometry.

References

Argyris, J.H., Scharpf, D.W., 1972. Large deflection analysis of prestressed networks. ASCE Journal of the Structural Division 98 (ST3), 633–654.

Bathe, K.-J., 1982. Finite Element Procedures In Engineering Analysis. Prentice-Hall, Englewood Cliffs, NJ.

Brillouin, L., 1964. Les Tenseurs en Mecanique et en Elasticite. Dover, New York.

Calladine, C.R., 1978. Buckminster Fuller's "Tensegrity" structures and Clerk Maxwell's rules for the construction of stiff frames. International Journal of Solids and Structures 14, 161–172.

Frankel, T., 1997. The Geometry of Physics, An Introduction. Cambridge University Press, Cambridge, MA.

Furuya, H., 1992. Concept of deployable tensegrity structures in space application. International Journal of Space Structures 7, 143–151.

Hanaor, A., 1993. Double-layer tensegrity grids as deployable structures. International Journal of Space Structures 8, 135–143.

Hughes, T.J.R., Pister, K.S., 1978. Consistent linearization in mechanics of solids and structures. Computers and Structures 8, 391–397.

Hughes, T.J.R., Winget, J., 1980. Finite rotation effects in numerical integration of rate constitutive equations arising in large-deformation analysis. International Journal for Numerical Methods in Engineering 15, 1862–1867.

Hughes, T.J.R., 1987. The Finite Element Method, Linear Static and Dynamic Finite Element Analysis. Prentice-Hall, Englewood Cliffs, NJ.

Ingber, D.E., 1998. The architecture of life. Scientific American, January, 2–11.

Koiter, W.T., 1984. On Tarnai's conjecture with reference to both statically and kinematically indeterminate structures. In: Report No. 788 of Laboratory of Engineering Mechanics, Delft University of Technology, Delft, Netherlands, pp. 3.

Marks, R., Fuller, R.B., 1973. The Dymaxion World of Buckminster Fuller. Anchor Books, Garden City, NY.

Marsden, J.E., Hughes, T.J.R., 1983. Mathematical Foundations of Elasticity. Prentice-Hall, Englewood Cliffs, NJ.

Maxwell, J.C., 1864. On the calculation of the equilibrium and stiffness of frames. Philosophical Magazine 27, 250.

Maxwell, J.C., 1890. In: Niven, W.D. (Ed.), The Scientific Papers of James Clerk Maxwell, Dover, New York, pp. 598–604.

Motro, R., 1990. Tensegrity systems and geodesic domes. International Journal of Space Structures 5, 341–351.

Murakami, H., Nishimura, Y., Impelluso, T.J., Skelton, R.E., 1998. A virtual reality-based CAD system for tensegrity structures. In: Murakami, H., Luco, J.E. (Eds.), Proceedings of the 12th ASCE Engineering Mechanics Conference, La Jolla, CA, pp. 197–200.

Pellegrino, S., Calladine, C.R., 1986. Matrix analysis of statically and kinematically indeterminate frameworks. International Journal of Solids and Structures 22, 409–428.

Przemieniecki, J.S., 1968. Theory of Matrix Structural Analysis. McGraw-Hill, New York (Chapter 15).

Pugh, A., 1976. An Introduction to Tensegrity. University of California Press, Berkeley, CA.

Schultz, D.G., 1981. Kenneth Snelson, an exhibition. Albright-Knox Art Gallery, Buffalo, NY, Thorney-Sidney Press, Buffalo, NY.

Skelton, R.E., Sultan, C., 1997. Controllable tensegrity, a new class of smart structures. SPIE, San Diego, pp. 12.

Tarnai, T., 1980. Simultaneous static and kinematic indeterminancy of space trusses with cyclic symmetry. International Journal of Solids and Structures 16, 347–359.